CrystEngComm

PAPER

View Article Online
View Journal | View Issue

Cite this: *CrystEngComm*, 2016, **18**, 2173

X-ray diffraction and computational studies of the pressure-dependent tetrachloroethane solvation of diphenylanthracene†

Francesca P. A. Fabbiani,*[a] Stefano Bergantin,[b] Angelo Gavezzotti,[c] Silvia Rizzato[c] and Massimo Moret*[b]

Received 8th January 2016,
Accepted 17th February 2016

DOI: 10.1039/c6ce00055j

www.rsc.org/crystengcomm

The crystal structure of the organic semiconductor 9,10-diphenylanthracene (DPA) has been studied by single-crystal X-ray diffraction at variable pressure up to 3 GPa. Under ambient conditions and in the presence of 1,1,2,2-tetrachloroethane, the material invariably crystallises in an unsolvated form, in the space group $C2/c$, with $Z' = 1/2$, as reported in the literature. As pressure is increased to a modest 0.5 GPa, crystallisation occurs in the form of a newly discovered solvate with a 1 : 2 DPA–tetrachloroethane stoichiometry, with the space group $P2_1/c$. A theoretical analysis by the PIXEL method with energy partitioning into Coulombic polarisation and dispersion terms reveals that the solvated and unsolvated structures have in common two basic packing motifs for the DPA molecule, one with linear interlocking and one with a T-shaped arrangement in a quincunx fashion. The solvent is enclosed in a cage and interacts with the DPA molecule by a very strong dispersive component of 44 kJ mol^{-1}. Monte Carlo simulations show that the mobility of the solvent in its cage would be extremely reduced even under ambient conditions, ruling out a mechanism of solvate formation and subsequent release. According to a structure-oriented perspective, the kinetics of the process could then be such that the nucleating system at ambient pressure separates out the solvent, while a 0.5 GPa pressure provides a solute–solvent grip that forces cocrystallisation, in agreement with both experiments and simulations. Even in the absence of experimental or computational proof of the thermodynamic stability of the solvate at high pressure, this appears to be a plausible and sensible case scenario in its own right.

1 Introduction

In recent years, the structural response of several polycyclic aromatic hydrocarbons (PAHs) to high pressure has been investigated experimentally, using both direct compression and *in situ* crystallisation techniques,[1–3] and computationally.[4,5] PAHs are currently attracting considerable interest because of their potential application as organic semiconductors in electronic and optoelectronic devices.[6] Most recently, we have investigated the organic semiconductor rubrene and obtained a high-pressure polymorph above 6.0 GPa; the structure, obtained by a reversible single-crystal-to-single-crystal transition, is characterised by a "double twisting" of the tetracene core and "scissoring" of the lateral phenyl groups, which are not observed in any of the ambient-pressure polymorphs.[3]

9,10-Diphenylanthracene (DPA) has recently attracted attention as an organic semiconductor with high electron and hole mobilities; the conducting mechanism is not fully understood but probably results from an effective intermolecular linking between successive layers inside the crystal, *via* the anthracene-backbone-phenyl-groups.[7] DPA crystallises in the space group $C2/c$ with the molecule residing on the centre of symmetry at ($\frac{1}{4}$, $\frac{1}{4}$, 0) and the two phenyl groups almost orthogonal (67.8°) to the anthracene backbone. Its ambient-pressure structure was first reported in 1979 (ref. 8) (CSD[9] reference code DPANTR) and later redetermined in 1992 (DPANTR01).[10] A 93 K study has been published recently[11] (DPANTR04). In 1975, Sloan reported in a private communication[12] that crystals grown from the melt crystallise in the space group $P2/m$, with a = 9.99 Å, b = 21.06 Å, c = 9.11 Å, β = 112° and Z = 4; however, no structural details are available and to the best of our knowledge this polymorph has not been identified in subsequent studies. Tripathi[13] reported that single crystals of a $P2/a$ polymorph

[a] *GZG, Abteilung Kristallographie, Georg-August-Universität Göttingen, Goldschmidtstr. 1, D-37077 Göttingen, Germany. E-mail: ffabbia@gwdg-de*
[b] *Dipartimento di Scienza dei Materiali, Università di Milano-Bicocca, Via R. Cozzi 55, 20125 Milano, Italy. E-mail: massimo.moret@unimib.it*
[c] *Dipartimento di Chimica, Università di Milano, via Golgi 19, 20133 Milano, Italy*

† Electronic supplementary information (ESI) available: Raman spectra, CheckCIF reports, packing, PIXEL energies and Monte Carlo simulations diagrams. CCDC reference numbers 1442973–1442975 contain the supplementary crystallographic data for this paper. For ESI and crystallographic data in CIF or other electronic format see DOI: 10.1039/c6ce00055j

with unit cell parameters a = 9.498 Å, b = 20.413 Å, c = 10.084 Å, β = 112.307° and Z = 4 can be obtained by sublimation; although no structural coordinates have been deposited with the CCDC for this form, inspection of packing diagrams available in the publication reveals that the structure most likely belongs to the space group $P2_1/a$ and contains two half molecules in the asymmetric unit. Very recently, in an elegant study, Salzillo *et al.* have reported the structures of two polymorphs of DPA obtained under kinetic control: a β-phase, corresponding to the form reported by Tripathi in the space group $P2_1/a$, and a γ-phase, crystallising in the space group $P2_1/n$.[14] Both polymorphs are less dense than the $C2/c$ one and hence would not be expected to preferentially form at high pressure. Two solvated forms (with hexafluorobenzene, CSD reference code MOGTAE, and 1,4-dioxane, MOGTEI), are known.[15] Unlike rubrene, DPA exhibits fairly good solubility in a variety of organic solvents; hence, we set out to investigate the structural response of DPA to high-pressure conditions, focussing on the study of solid forms obtained by *in situ* high-pressure crystallisation and hoping to alter the molecular conformation by the application of modest (<1.0 GPa) pressures.

2 Experimental

A diamond-anvil cell (DAC) based on the Merrill-Bassett design[16] equipped with Be backing plates was used for the *in situ* crystallisation experiment. This cell was also used for the 3 GPa data point in the compression study; for the 0.5 GPa data point, a Be-free DAC based on a square-shaped DAC of the Ahsbahs type[17] was employed. Both cells were equipped with 600 μm culet diamonds and Inconel 718 gaskets with a 250 μm hole. The DAC had a half-cell opening angle of 40°. The ruby fluorescence method[18] was used for pressure calibration using an in-house built kit that has a precision of 0.05 GPa.

2.1 *In situ* crystallisation from DPA-1,1,2,2-tetrachloroethane

Toluene, *p*-xylene and *m*-xylene and their mixtures, and 1,1,2,2-tetrachloroethane were screened as solvents for preparing DPA solutions for *in situ* high-pressure crystallisation. No crystallisation of DPA was observed in toluene (*ca.* 0.15 M solution) and the ambient-pressure unsolvated form of DPA was obtained from *p*-xylene (*ca.* 0.2 M solution) and from a 7 : 1 *m*-/*p*-xylene mixture (*ca.* 0.3 M). In 1,1,2,2-tetrachloroethane, appreciable solubility could be reached. A *ca.* 0.4 M solution (corresponding to *ca.* 8% w/w) was loaded in the DAC and the pressure was increased to just below the freezing point of the neat solvent, *ca.* 0.5 GPa.[19] The DAC was subsequently kept at 278 K for 24 hours; this procedure resulted in the crystallisation of both the solvent and a DPA-containing form, identified by single-crystal X-ray diffraction as the disolvate, here termed DPA-S, which could be dissolved *in situ* at high pressure by temperature cycling at *ca.* 353 K to grow a single crystal (Fig. 1). The final pressure inside the DAC was recorded as *ca.* 0.5 GPa. Ambient-pressure crystallisation from the same solution invariably resulted in the crystallisation of the known unsolvated form of DPA. Low-temperature crystallisation experiments of DPA from 1,1,2,2-tetrachloroethane were additionally carried out in order to verify whether the high-pressure solvate could also be obtained *via* an ambient-pressure crystallisation route. Several crystallisation experiments were performed using an Oxford Cryosystem 700 Plus liquid nitrogen low-temperature device mounted on a Rigaku R-Axis Rapid II diffractometer equipped with a SHINE monochromator (Mo Kα radiation, λ = 0.71075 Å) and an image plate detector. Flash cooling experiments led to the formation of an amorphous material and microcrystals of 1,1,2,2-tetrachloroethane, as identified by X-ray diffraction. Heating past the melting point of the solvent (229 K), resulted in complete dissolution of the material.

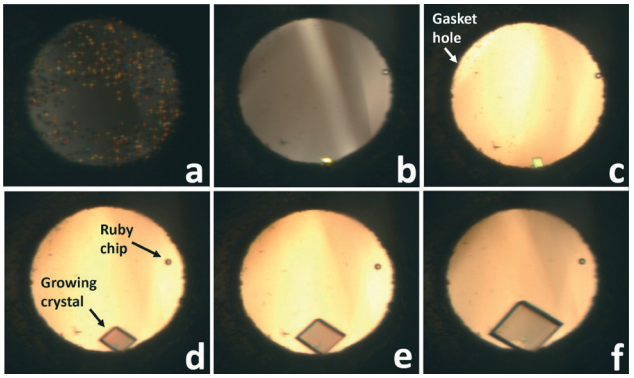

Fig. 1 Stages of crystal growth of DPA-1,1,2,2-tetrachloroethane solvate (DPA-S) in a DAC. DAC diameter = 250 μm. a) Precipitation of polycrystalline material; b) single crystal grain after temperature cycling; c–f) stages of crystal growth on cooling to ambient temperature.

2.2 Compression study of DPA

A single crystal of DPA grown from 1,1,2,2-tetrachloroethane was loaded in the DAC using a 4 : 1 MeOH/EtOH solution as a pressure-transmitting medium. Raman spectra were collected at 0.03 GPa intervals up to 3.0 GPa using a Horiba Jobin Yvon HR800 UV Micro-Raman spectrometer equipped with an air-cooled 325 mW 785 nm diode laser. This particular laser was chosen in order to minimise the otherwise considerable fluorescence signal from the sample. The Raman spectra were collected in the 150–1800 cm^{-1} range with a spectral resolution of *ca.* 2.2 cm^{-1} using a grating of 600 grooves per mm and a Peltier-cooled CCD detector (Andor, 1024 × 256 pixels). No phase transition was observed up to 3.0 GPa. The Raman spectra have been deposited in the ESI.† At this pressure, single-crystal X-ray data were collected. The single crystal was not subjected to further compression. The compression study was performed primarily to rule out the occurrence of a phase transition at pressures similar to those at which the solvate was observed. In this respect, the choice of the upper limit of compression was not dictated by loss of data quality. A more comprehensive compression study should be the

subject of a future investigation. In a subsequent experiment, a single crystal of DPA grown from 1,1,2,2-tetrachloroethane was compressed up to 0.5 GPa and single-crystal X-ray data were collected at this pressure.

2.3 X-ray crystallography

Single-crystal diffraction data were collected on a Bruker APEX II CCD diffractometer at 293(2) K using Mo Kα radiation (λ = 0.71073 Å). Data collection and processing were performed according to procedures described by Dawson *et al.*[20] Data were collected using a combination of ω and ϕ scans to maximise data completeness and redundancy. For the DPA-S, diffraction data were collected with the DAC in three orientations to simulate three different values of χ in order to improve data completeness. For the compression study of DPA at 0.5 and 3.0 GPa, data were collected with the DAC in either two or single orientation, respectively.

A non-standard monoclinic setting for the structure of DPA at 0.5 and 3.0 GPa was chosen to enable a direct structural comparison with the ambient-pressure, ambient-temperature structure (DPANTR01). Data integration and global-cell refinement were performed using the program SAINT[21] in conjunction with dynamic masks to exclude the regions of the detector shaded by the pressure cell.[20] Additional masks for the three most intense powder rings (100, 002 and 101) from the beryllium backing discs were used. Absorption corrections were then applied in a two-stage procedure with the programs SHADE[22] and SADABS.[23] Data were merged using the program SORTAV,[24] as incorporated in the WinGX suite.[25] The structure of the solvate was easily solved with SHELXT.[26] Full-matrix least-squares structure refinement against F^2 was performed using SHELXL[27] through the SHELXLE GUI.[28] ADPs were restrained by means of enhanced rigid-body restraints[29] to obtain a satisfactory model. U_{iso}(H) values were assigned in the range 1.2–1.5 times U_{eq} of the parent atom. Stereochemical 1,2-distances (DFIX) and 1,3-distances (DANG) restraints were applied to increase the robustness of the refinement: restraints were generated by the GRADE Web server (http://grade.globalphasing.org). A GRADE dictionary for SHELXL contains target values and standard deviations for 1,2-distances (DFIX) and 1,3-distances (DANG), as well as restraints for planar groups (FLAT), which were not used in our case. Final *R*-factors in the range of 4.5% for all structures testify to the good structural quality. Further crystallographic details are given in Table 1 and are available in the CIF deposited in the ESI.†

3 Computational methods

Crystal lattice energies and molecule–molecule energies with separate Coulombic-polarisation and dispersion contributions have been calculated by the PIXEL approach.[30] For the Monte Carlo (MC) simulations of crystal structures, intermolecular energies have been calculated in the atom–atom CLP formalism;[31] the DPA molecule was modelled with the geometry extracted from the X-ray determination under room conditions (CSD refcode DPANTR01) with a rigid anthracene core and two rigid phenyl rings, the only intramolecular degrees of freedom being thus the two implied torsion angles. The corresponding torsional energy profile was analysed in 1-phenylanthracene, obtained from DPA by replacing one phenyl ring with a hydrogen atom. The total molecular energy was calculated by *ab initio* calculation at the MP2/6-31G level as a function of τ and fitted by a fourth-order polynomial (Fig. 2). The MC computational crystal box was built from 4 × 3 × 3 cell replications, giving box sides of 35–40 Å and comprising 144 molecules, with periodic boundary

Table 1 Crystallographic data for DPA structures discussed in this paper

			DPA	DPA	DPA-S
Structure	DPANTR01	DPANTR04	CCDC 1442974	CCDC 1442975	CCDC 1442973
Formula	$C_{26}H_{18}$	$C_{26}H_{18}$	$C_{26}H_{18}$	$C_{26}H_{18}$	$C_{26}H_{18}{\cdot}2(C_2H_2Cl_4)$
Molecular weight	330.42	330.42	330.42	330.42	666.07
Space group	*C*2/*c*	*C*2/*c*	*C*2/*c*	*C*2/*c*	$P2_1/c$
a, *b*, *c*/Å	10.683(4), 13.552(2), 12.257(2)	10.5768(10), 13.5065(13), 12.0761(12)	10.4702(9), 13.3923(10), 12.0158(11)	10.041(2), 13.150(2), 11.378(2)	8.7874(3), 12.0308(7), 13.8215(8)
β/°	90.54(2)	90.1200(10)	89.931(8)	88.483(17)	104.964(3)
V/Å^3	1774.4(8)	1725.1(3)	1684.9(2)	1501.8(5)	1411.65(13)
Z′	0.5	0.5	0.5	0.5	0.5
D_{calc}/g cm^{-3}	1.237	1.272	1.303	1.461	1.567
Pressure	0.1 MPa	0.1 MPa	0.5 GPa	3.0 GPa	0.5 GPa
T/K	298	93	296(2)	296(2)	296(2)
Torsion τ/°	67.79(9)	66.50(4)	65.87(9)	62.3(2)	83.2(4)
Meas./uniq./obs. reflections			6071, 937, 765	1704, 422, 308	8102, 650, 504
θ_{max}/°			25.3	19.8	17.3
Completeness to θ_{max}/%			60.3	61.4	75.4
R_{int}			0.020	0.042	0.048
$R[F^2 > 2\sigma(F^2)]$, w$R(F^2)$, *S*			0.037, 0.095, 1.10	0.053, 0.148, 1.06	0.052, 0.131, 1.06

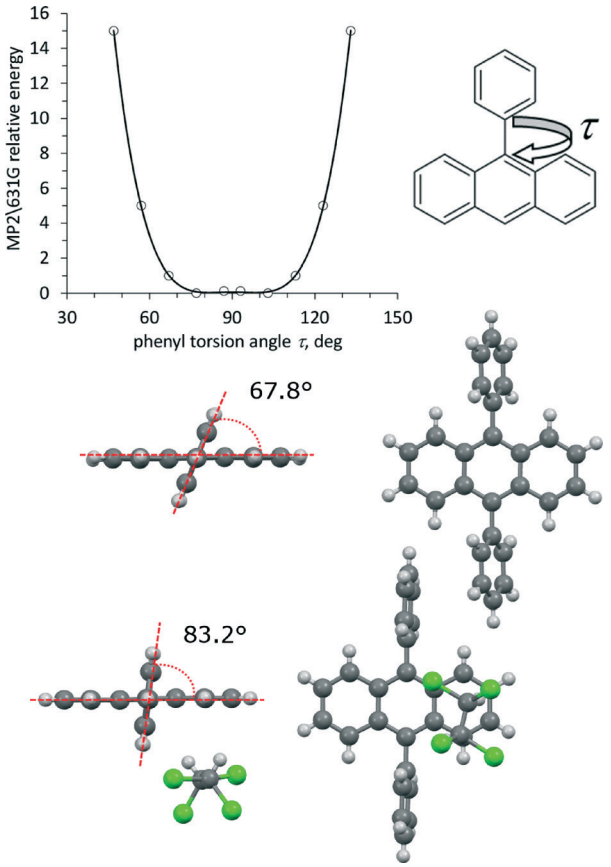

Fig. 2 Top: The MP2/6-31G energy profile (kJ mol^{-1}) for torsion, τ, of the phenyl group in phenylanthracene. Bottom: Torsion angles for DPA and for DPA-S.

conditions. Pressure control was implemented under the standard Isothermal–Isobaric Ensemble (IIE) conditions. More detail on methods and software description and availability can be found in the original reference.[32] MC runs of 3 million steps each, including equilibration and production to ensure proper convergence to a stationary state, were performed at 293 K and variable pressure from 0.001 to 70 kbar. The resulting trajectories were analysed in the production sections in terms of average configurational total energies, average densities, and radial density functions defined in the usual way.[32] The source code and documentation of the software used can be found at the site www.angelogavezzotti.it, the link to the CLP-MC package.

4 Results and discussion

No phase transition for pristine DPA was observed on compressing a single crystal specimen up to 3 GPa. The new solvated form, DPA-S, crystallises in the space group $P2_1/c$ with the hydrocarbon molecule residing on the inversion centre, giving a stoichiometry of one molecule of DPA for two solvent molecules. The crystal packing of both forms, considering both structural and energetic aspects, is compared in more detail in the following sections.

4.1 Structural and energetic features

A crucial conformational feature of the DPA molecule is obviously the angle between the planes of the anthracene core and the lateral phenyl rings, as described by one C–C–C–C torsion angle τ (<90°). In the structure of DPA at ambient temperature and pressure, this value is 67.79(9)° (Table 1). As the structure is compressed, τ decreases reaching a minimum of 62.3(2)° at 3.0 GPa, as the molecule adjusts by becoming flatter. Fig. 2 shows that the phenyl torsion angle can vary almost freely (that is, within an energy window of RT, 2.5 kJ mol^{-1} under room conditions) between 60 and 90°. Accordingly, in the solvate the angle rises to 83.2(4)° at almost no energy expense, clearly prompted by the need to make more room available for the solvent molecule by widening the channel (see below).

The total lattice energies for DPA, calculated by the PIXEL method and reported in Table 2, indicate the expected destabilisation with increasing pressure (stabilisation or destabilisation refer to energies becoming more negative or less negative, respectively). In DPA, the destabilisation arises from the very steep repulsive contribution, while dispersive contributions become more and more stabilising at shorter distances, as they should.

The Coulomb and dispersion energy terms of the DPA–DPA interaction show a large destabilisation on going from the pristine to the solvate structure at 0.5 GPa. This is more than compensated by the very large DPA–solvent dispersive contribution, predictably due to the interaction between the polarisable outer electrons of chlorine and polarisable π-electrons. The solvate is thus mostly stabilised by hydrocarbon–solvent interactions. Solvent–solvent interactions are an order of magnitude smaller than the other two contributions, also as expected because their close contact is screened by the large solute molecule. On the other hand, lowering the temperature causes the expected stabilisation of the lattice energy due to the closer contact between molecules with cell shrinkage. Thus, the PIXEL analysis in partitioned terms clearly shows and explains the essential physical phenomena occurring with variations in temperature and pressure.

More revealing than the total lattice energies is the analysis of individual molecule–molecule contacts. Coordination motifs are thus drawn by selecting the molecular partners with the highest contact energy, this being an objective physicochemical criterion as opposed to the subjective visual inspection of short atom–atom distances or supposed "weak" bonds. The energy values are collected in Tables 3 and 4 and in Fig. S3,† while molecular diagrams are in Fig. 3 and 4. The solvate structure DPA-S is mostly stabilised by solvent–solute interactions, as seen from motifs D and E in Table 4. Besides, DPA and DPA-S have in common the two main cohesive motifs A and C: motif A is formed by steric interlocking of the side phenyl rings and core anthracene moiety, while motif C is a herringbone-type, T-shaped arrangement so common in the crystal structures of condensed aromatics.[33] In the solvate structure these two motifs are distorted by the presence of

Table 2 Lattice energies (PIXEL values) in kJ mol^{-1} of the DPA and DPA-S structures, partitioned between the solute and solvent where appropriate

		E_{coul}	E_{pol}	E_{disp}	E_{rep}	E_{tot}	
DPANTR01	295 K	−31.4	−16.3	−193.9	93.4	−148.2	
DPANTR04	93 K	−39.9	−22.3	−215.8	53.8	−154.1	
DPA	0.5 GPa	−45.1	−24.2	−218.1	143.5	−143.9	
DPA	3.0 GPa	−103.7	−60.5	−313.9	352.0	−126.1	
DPA-S	0.5 GPa	−22.3	—[a]	−92.9	59.1	—	DPA–DPA
		−70.0	—	−310.6	180.3	—	DPA–solvent

[a] The polarisation energy is a many-body term and cannot be partitioned over the solute and solvent.

Table 3 Structure-determining molecular pairs in the crystal structure of DPANTR01 at ambient temperature and pressure as determined by PIXEL calculations. Energies in kJ mol^{-1}

Symmetry operator and translation vectors[a]	Motif[b]	R(c.o.m.)[c]	E_{coul}	E_{pol}	E_{disp}	E_{rep}	E_{tot}[d]
CT [($\frac{1}{2}$, $\frac{1}{2}$, 0); ($-\frac{1}{2}$, $-\frac{1}{2}$, 0)]	A	8.628	−8.9	−4.0	−38.7	27.2	2(−24.3)
CT [($-\frac{1}{2}$, $\frac{1}{2}$, 0); ($\frac{1}{2}$, $-\frac{1}{2}$, 0)]	B	8.628	−5.5	−2.1	−28.5	11.8	2(−24.3)
RO ($\frac{1}{2}$, $\pm\frac{1}{2}$, $\pm\frac{1}{2}$)	C	9.136	−5.9	−3.0	−30.4	16.0	4(−23.2)
RO [(1, 0, $-\frac{1}{2}$); (0, 0, $\frac{1}{2}$)]		8.167	0.0	−1.2	−27.7	8.2	2(−20.7)

[a] Symmetry labels: CT: centering vector; RO: 2-fold rotation axis along b. [b] See Fig. 3. [c] Distance in Å from the centre of mass of the central molecule to the centre of mass of the surrounding ones. [d] The integer number preceding E_{tot} refers to the multiplicity of the interaction.

Table 4 Structure-determining molecular pairs in the crystal structure of DPA-S at 0.5 GPa as determined by PIXEL calculations. Energies in kJ mol^{-1}

Symmetry operator and translation vectors[a]	Motif[b]	R(c.o.m.)[c]	E_{coul}	E_{pol}	E_{disp}	E_{rep}	E_{tot}[e]
DPA–DPA							
T (±1, 0, 0)	A	8.787	−7.5	−3.4	−34.3	22.4	2(−22.8)
S [(−1, $\pm\frac{1}{2}$, $-\frac{1}{2}$); (1, $\pm\frac{1}{2}$, $-\frac{3}{2}$)]	C	9.162	−7.0	−3.5	−26.4	18.4	4(−18.5)
DPA–solvent 1[d]							
S (0, $-\frac{1}{2}$, $-\frac{1}{2}$)	D	4.828	−7.5	−11.4	−50.6	34.7	−44.9
T (−1, 0, −1)	E	6.959	−6.9	−4.2	−34.2	22.3	−23.0
S (−1, $-\frac{1}{2}$, $-\frac{1}{2}$)	F	7.269	−3.4	−2.5	−27.9	13.9	−19.9

[a] Symmetry labels: T: identity (pure translation); S: 2-fold screw axis along b. [b] See Fig. 4 and 6. [c] Distance in Å from the centre of mass of the central molecule to the centre of mass of the surrounding ones. [d] Each term has a corresponding term to solvent 2. [e] The integer number preceding E_{tot} refers to the multiplicity of the interaction.

the solvent, and are therefore less stabilising than in the pristine structure (especially the C motif) as can be seen on close comparison of Fig. 3 and 4, and as confirmed by the slightly longer centre-of-mass separations (8.78 and 9.16 against 8.63 Å).

The fact that the two structures have an overall frame in common is also evident in Fig. 5, which shows that the pristine structure has a sort of predisposition to forming alignments (channels) of solvates. In other words, the arrangement of the molecules in the (100) plane of DPA-S is similarly present in the first (100) layer of the structure of DPA. DPA and DPA-S have in fact almost identical b and c axes, but a different orientation of the cell (the axes are swapped in the two structures, see Table 1 and Fig. S2 in the ESI†). The widening of the β angle in DPA-S (formerly $\gamma = 90°$ in DPA) together with the length reduction of the a-axis

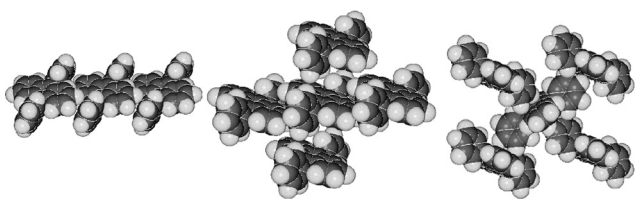

Fig. 3 Structural motifs formed by the three most stabilising molecular pairs in the unsolvated DPA crystal. Left: A motif; middle: A motif (horizontal) + B motif (vertical); right: C motif. See Table 3 for details.

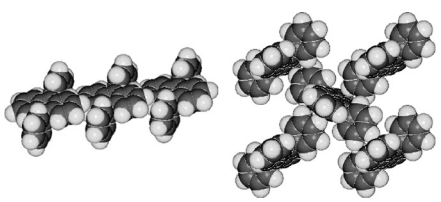

Fig. 4 Structural motifs involving DPA molecules in the structure of DPA–S. Left: A motif; right: C motif, as in Fig. 3. See Table 4 for details.

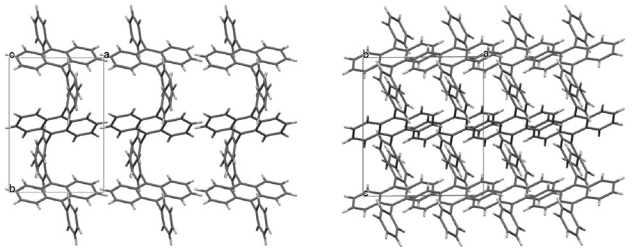

Fig. 5 Left: The crystal structure of DPA-S shown with empty solvent channels seen along *c*. Right: Wireframe projection of unsolvated DPA seen along *b*.

prevent the formation of the second layer of DPA molecules, which is replaced by solvent molecules.

The coordination modes between DPA and the solvent in the structure of DPA-S are shown in Fig. 6. From the point of view of the solute DPA molecule, it is seen to be surrounded by six nearest-neighbour solvent molecules (Table 4), one above and one below the main anthracene core (this is the most cohesive coupling), and four coordinating to each side of the two lateral phenyl rings. Seen from the opposite end, one solvent molecule is fully encapsulated by lateral phenyl rings and by the external rings of the anthracene core. What look like channels in Fig. 5 are in fact translational sequences of coordination cages, whose grip is presumably sensitive to pressure, allowing enough fluctuation to allow their escape at ambient pressure but preventing solvent molecules from leaving at 0.5 GPa.

4.2 Monte Carlo simulations

Fig. 7 shows that the radial distribution function of the centre of mass, $g(R)$, is broad at ambient pressure, with a peak overlap in the 7.5–9.5 Å region, corresponding to the structure determinants shown in Table 3. As pressure increases, all peaks shift to shorter distances, as expected, and separate peaks appear due to the reduced molecular mobility. At room pressure, the broad distribution of phenyl torsion angles peaks at 65°, and falls to zero at 50°. At high pressure, the distribution is narrower and peaks at 61° as the molecule becomes flatter to comply with the external stimulus. The minimum value, around 50°, does not decrease further for obvious steric reasons.

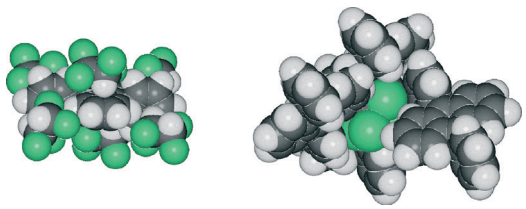

Fig. 6 DPA-S crystal. Left: Solute–solvent coordination in the D, E and F motifs, refer to text and Table 4 for details; solvent molecules are related in pairs by a centre of symmetry. Right: The cage formed by the hydrocarbon molecules around a solvent molecule.

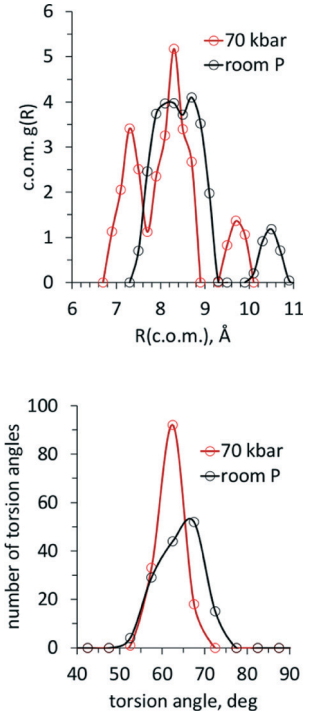

Fig. 7 Results of the Monte Carlo simulations for the DPA crystal. Top: Centre-of-mass radial density function, $g(R)$. Bottom: Distribution of phenyl torsion angles.

Fig. 8 shows the equations of state of the material, as resulting from our MC simulations. The bulk moduli at zero pressure, B_0, and their derivative B', obtained by fitting a

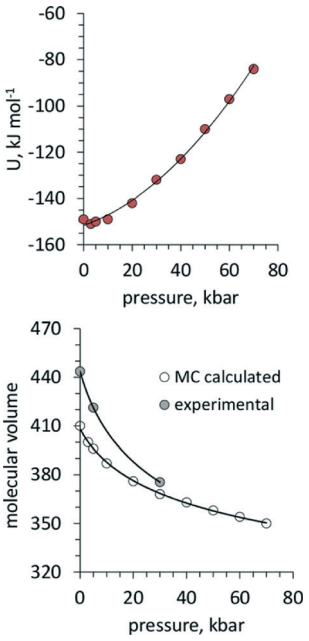

Fig. 8 Top: Total configurational energy (kJ mol^{-1}), data fitted to $y = 0.0089x^2 + 0.3611x - 151.58$; bottom: molecular volume (Å^3, open circles calculated, filled circles experimental) for DPA as a function of pressure. Data fitted to a Murnaghan equation of state, see text for details.

Murnaghan equation of state using EosFIT7 GUI[34] to the MC and experimental data, are 13 GPa and 14, and 7.53(3) GPa and 9.27(6), respectively. Given the limited number of data points, these numbers should be interpreted with caution and in no case used for extrapolation to higher pressures. Nevertheless, it becomes apparent that the resulting values are quite in line with those found for other aromatic hydrocarbons, *e.g.* 8.21(84) GPa and 9.37(89) for triclinic rubrene,[35] 8.4(6) GPa and 6.3(4) for anthracene,[36] 9.0(20) GPa and 7.9(12) for tetracene[36] and 9.6(10) GPa and 6.4(5) for pentacene.[36] The simulation underestimates the molecular volume at zero pressure by about 7%, a discrepancy well within the usual range for force field calculations. There is a better agreement with the single experimental data point at 30 kbar, while the trends suggest a slight overestimation at higher pressures. The experimental value of the thermal expansion coefficient $(1/V)(\mathrm{d}V/\mathrm{d}T)$ from the cell volumes of the two crystal structures at 293 and 93 K is 1.4 10^{-4} K^{-1}, quite in line with normal values for organic crystals.[37] The $U(T)$ curve has no immediate experimental counterpart for comparison. The MC total energy is potential energy only, but to a first approximation the kinetic energy part of the internal energy is independent of pressure, so that we take the MC total configurational energy as the total internal energy, U. The pressure coefficient derived from the U/P plot from the MC simulations is $\mathrm{d}U/\mathrm{d}P = 0.0178P + 0.361$ kJ mol^{-1} $kbar^{-1}$, or 6.3 10^{-6} m^3 mol^{-1} at $P = 15$ kbar. This value can be checked indirectly against the experimental one, as follows. Given the thermodynamic identity $(\mathrm{d}U/\mathrm{d}P)_T = -T(\mathrm{d}V/\mathrm{d}T)_P - P(\mathrm{d}V/\mathrm{d}P)_T$, one can introduce the experimental values for the thermal expansion and compressibility coefficients, for the average temperature and pressure (in appropriate units, 3.6×10^{-8} m^3 K^{-1} mol^{-1} and -1.12×10^{-6} m^3 $kbar^{-1}$ mol^{-1}, 200 K and 15 kbar in the respective intervals). With these data $\mathrm{d}U/\mathrm{d}P = -200 \times 3.6\ 10^{-8} + 15 \times 1.12\ 10^{-6} = 9.6 \times 10^{-6}$ m^3 mol^{-1}, in reasonable agreement with the calculated value of 6.3 10^{-6} m^3 mol^{-1}.

The above results show that our MC simulations are not too far from reality. However, these simulations are not accurate enough to provide clues as to the relative thermodynamic stability of the solvate phase as a function of pressure. From a structure-oriented perspective, one might invoke a kinetic effect with a temporary opening of the solvent cages at the crystal surface, allowing solvent escape at room pressure, which becomes blocked by tighter packing at higher pressure. Probing this hypothesis by molecular simulation is a challenging task. Standard simulations of the bulk solvate crystal indicate a very limited mobility of the solvent already at room pressure, with a root-mean-square displacement of the order of just 0.2 Å. The final frame of an ambient-pressure simulation was used a starting point for a 10-million step simulation run without periodic boundary conditions, thus exposing the solvate molecules at the crystal surface but preventing pressure control. Not even these conditions could reveal any significant displacement of solvent molecules (see Fig. S4, ESI,† for a snapshot of the final frame, showing ordered solvent molecules except for thermal oscillations). This result is presumably a consequence of the very high solute–solvent cohesive energy shown in Table 4.

5 Conclusions

The crystal structure of DPA has been studied by single-crystal X-ray diffraction at pressures up to 3 GPa. A 1 : 2 DPA-1,1,2,2-tetrachloroethane solvate (DPA-S) has been obtained by *in situ* high-pressure crystallisation from solution. The finding that DPA-S can only be obtained at high pressure is somewhat surprising, although not entirely new;[38–41] besides, the existence of a DPA solvate at ambient pressure cannot be entirely ruled out. Quench-cooling experiments, followed by temperature annealing, perhaps coupled with an IR laser, zone-melting procedure,[42] which offers much better temperature and spatial control, would be necessary to further assess this point. Such experiments have been useful in obtaining crystalline phases that are highly metastable at ambient temperature and pressure.[43,44] Further efforts in this direction could involve lowering the temperature or using more concentrated solutions. The ensuing experiments would presumably require very high investment in time and resources, for a very uncertain promise.

The solvated and unsolvated crystal structures have in common two basic packing motifs, one with linear interlocking and one with a T-shaped arrangement of DPA solute molecules. A theoretical PIXEL analysis shows that these are the most stabilizing structural motifs. The solvent is enclosed in a cage, and the PIXEL analysis reveals that it interacts with the surrounding DPA molecules by a strong stabilizing energy of entirely dispersive nature. Variable-pressure Monte Carlo simulations using the CLP atom–atom force field reproduce reasonably well the experimental crystal structures and densities up to 3 GPa, and provide an acceptable estimate of the pressure coefficient of internal energy. More importantly, the simulations clearly show that the mobility of the solvent in its cage is extremely reduced even under ambient conditions, negating a mechanism in which the solvent is incorporated and subsequently released.

Notwithstanding these positive results, our simulations neither prove nor disprove a relative thermodynamic stability as a function of pressure. Basic thermodynamic relationships, $(\mathrm{d}G/\mathrm{d}P)_T = V$, prescribe an increase in free energy with increasing internal pressure, at least for a one-component system. Increased thermodynamic stability with increasing pressure could however arise in binary systems from differential enthalpies of solvation. This seems to be the case for GABA monohydrate[38] where periodic DFT calculations at 0 K showed that at high pressure the enthalpy of hydration becomes increasingly more negative. GABA monohydrate can be recovered under ambient-pressure conditions, and used for seeding, because under these conditions it is energetically close to the anhydrous polymorph plus ice. As already mentioned, unfortunately DPA-S could not be recovered under ambient conditions, at least as far as our present experimental work goes.

There has been so far no answer to the essential question: is the solvate stable only under pressure, and if so, why. In summary, there is neither experimental nor computational proof of the thermodynamic stability of DPA-S at high pressure. Cocrystallisation energies of *ca.* −11 kJ mol^{-1} have been reported for molecular organic materials at ambient pressure,[45] an order of magnitude that does not seem to pose forbidding thermodynamic obstacles. Thus, a sensible hypothesis involves the kinetic control of pore opening that would allow the escape of solvent molecules either for the preformed crystal or, more likely, at the nucleation stage, but only under ambient conditions. An external pressure could provide a mechanical grip that would ensure the retention of solvents. This scenario sidesteps all thermodynamic arguments, and is also supported by the results of the Monte Carlo simulation of the surface of a crystal slab. High-pressure crystallisation under kinetic control is well documented;[46] for instance, polymorphism dependent on the compression rate has been demonstrated for 2-fluorophenylacetylene,[47] a liquid at ambient pressure, and for L-serine.[48] A 7.6-fold increase in growth rate for glucose isomerase was observed at 0.1 GPa, due to kinetic factors.[49] Seeding effects in nucleation kinetics could arise from the rough surfaces of the sample chamber or the ruby chip used as a pressure calibrant; in the case of DPA-S, potential seeding points were provided by crystallisation of the solvent, with crystals acting as nucleants. Finally, one should mention the possibility of speeding or altering the nucleation process by generating supersaturation on increasing pressure, as a result of the accompanying volume reduction inside the pressure cell.

Crystal form selection and control is an area of intense research activity, and the thermodynamic-kinetic divide is at the heart of the matter: "the crystal energy landscape usually includes many more structures than experimentally observed polymorphs. Understanding why, in terms of kinetics of crystallisation, is the main challenge to polymorph prediction."[50] From a thermodynamic point of view, progress has been made by estimating the vibrational contribution to free energy[51] or by taking into account the configurational contribution to the lattice free energy in disordered structures.[52] Kinetic effects are beginning to be tackled by appropriate use of adapted molecular dynamics.[53,54] The task is by no means trivial but a better understanding of nucleation and growth kinetics is indispensable; the formation of crystal phases exclusively or preferably at high pressure is a piece in the mosaic. Experiments are hampered by the size- and timescale of the problem. Computations are becoming more and more accessible to the wider structural chemistry community. Progress will in general require the use of wise combinations of both.

Acknowledgements

M. Moret and S. Bergantin are grateful to Fondazione Cariplo (Grant No. 2009/2551) for financial support. F. P. A. Fabbiani thanks the DFG for funding, Emmy Noether project FA 9649/1-1, as well as Ulf Kahmann and Heiner Bartels (University of Göttingen) for technical support, and Rubén Granero-García (University of Göttingen) for useful discussions. Fig. 3, 4 and 6 were drawn with the help of the program SCHAKAL by Egbert Keller (University of Freiburg).

References

1 F. P. A. Fabbiani, D. R. Allan, S. Parsons and C. R. Pulham, *Acta Crystallogr., Sect. B: Struct. Sci.*, 2006, **62**, 826.
2 F. P. A. Fabbiani, D. R. Allan, W. I. F. David, S. A. Moggach, S. Parsons and C. R. Pulham, *CrystEngComm*, 2004, **6**, 504.
3 S. Bergantin, M. Moret, G. Buth and F. P. A. Fabbiani, *J. Phys. Chem. C*, 2014, **118**, 13476.
4 B. Schatschneider, S. Monaco, A. Tkatchenko and J.-J. Liang, *J. Phys. Chem. A*, 2013, **117**, 8323.
5 B. Schatschneider, S. Monaco, J.-J. Liang and A. Tkatchenko, *J. Phys. Chem. C*, 2014, **118**, 19964.
6 J. E. Anthony, *Angew. Chem., Int. Ed.*, 2008, **47**, 452.
7 A. K. Tripathi, M. Heinrich, T. Siegrist and J. Pflaum, *Adv. Mater.*, 2007, **19**, 2097.
8 J. M. Adams and S. Ramdas, *Acta Crystallogr., Sect. B: Struct. Sci.*, 1979, **35**, 679.
9 F. H. Allen, *Acta Crystallogr., Sect. B: Struct. Sci.*, 2002, **58**, 380.
10 V. Langer and H.-D. Becker, *Z. Kristallogr.*, 1992, **199**, 313.
11 Y. Fujiwara, R. Ozawa, D. Onuma, K. Suzuki, K. Yoza and K. Kobayashi, *J. Org. Chem.*, 2013, **78**, 2206.
12 G. Sloan, Personal communication to J. M. Thomas, 1975, cited in ref. 7.
13 A. K. Tripathi, *PhD Thesis (Dissertation)*, Universität Stuttgart, 2009, http://elib.uni-stuttgart.de/opus/volltexte/2009/3746/.
14 T. Salzillo, R. G. Della Valle, E. Venuti, A. Brillante, T. Siegrist, M. Masino, F. Mezzadri and A. Girlando, *J. Phys. Chem. C*, 2016, **120**, 1831.
15 Y. Imai, K. Kawaguchi, T. Sato, N. Tajima, R. Kuroda and Y. Matsubara, *Mol. Cryst. Liq. Cryst.*, 2008, **487**, 153.
16 L. Merrill and W. A. Bassett, *Rev. Sci. Instrum.*, 1974, **45**, 290.
17 H. Ahsbahs, *Z. Kristallogr.*, 2004, **219**, 305; H. Ahsbahs, 20 Jahre Merrill-Bassett-Zelle. Einige Neuheiten., *Z. Kristallogr. Suppl.*, 1995, **9**, 42.
18 G. J. Piermarini, S. Block, J. D. Barnett and R. A. Forman, *J. Appl. Phys.*, 1975, **46**, 2774.
19 M. Bujak and A. Katrusiak, *Z. Kristallogr.*, 2004, **219**, 669.
20 A. Dawson, D. R. Allan, S. Parsons and M. Ruf, *J. Appl. Crystallogr.*, 2004, **37**, 410.
21 *Bruker-Nonius, SAINT version 7.32A*, Bruker-AXS, Madison, Wisconsin, USA, 2006.
22 S. Parsons, *SHADE*, The University of Edinburgh, Edinburgh, United Kingdom, 2004.
23 G. M. Sheldrick, *SADABS Version 2012/1*, Bruker-AXS, Madison, Wisconsin, USA, 2004.
24 R. H. Blessing, *Acta Crystallogr., Sect. B: Struct. Sci.*, 1995, **51**, 33.
25 L. J. Farrugia, *J. Appl. Crystallogr.*, 1999, **32**, 837.

26 G. M. Sheldrick, *Acta Crystallogr., Sect. A: Found. Adv.*, 2015, **71**, 3.
27 G. M. Sheldrick, *Acta Crystallogr., Sect. C: Struct. Chem.*, 2015, **71**, 3.
28 C. B. Hübschle, G. M. Sheldrick and B. Dittrich, *J. Appl. Crystallogr.*, 2011, **44**, 1281.
29 A. Thorn, B. Dittrich and G. M. Sheldrick, *Acta Crystallogr., Sect. A: Found. Crystallogr.*, 2012, **68**, 448.
30 A. Gavezzotti, *Mol. Phys.*, 2008, **106**, 1473.
31 A. Gavezzotti, *New J. Chem.*, 2011, **35**, 1360.
32 A. Gavezzotti, *New J. Chem.*, 2013, **37**, 2110.
33 A. Gavezzotti, *Acta Crystallogr., Sect. B: Struct. Sci.*, 1988, **44**, 427.
34 R. J. Angel, J. Gonzalez-Platas and M. Alvaro, *Z. Kristallogr.*, 2014, **229**, 405.
35 S. Bergantin, M. Moret, G. Buth and F. P. A. Fabbiani, *J. Phys. Chem. C*, 2014, **118**, 13476.
36 M. Oehzelt, A. Aichholzer, R. Resel, G. Heimel, E. Venuti and R. D. Valle, *Phys. Rev. B: Condens. Matter Mater. Phys.*, 2006, **74**, 104103.
37 A. Gavezzotti, *Molecular Aggregation*, Oxford University Press, 2nd edn paperback, 2013, pp. 276 and 282.
38 F. P. A. Fabbiani, G. Buth, D. C. Levendis and A. J. Cruz-Cabeza, *CrystEngComm*, 2014, **50**, 1817.
39 S. Saouane and F. P. A. Fabbiani, *Cryst. Growth Des.*, 2015, **15**, 3875.
40 H. Tomkowiak, A. Olejniczak and A. Katrusiak, *Cryst. Growth Des.*, 2013, **13**, 121.
41 W. Zieliński and A. Katrusiak, *CrystEngComm*, 2015, **17**, 5468.
42 R. Boese and M. Nussbaumer, in *In Situ Crystallisation Techniques in Organic Crystal Chemistry*, ed. D. W. Jones, Oxford University Press, Oxford, 1994, pp. 20–37.
43 N. V. Surovtsev, S. V. Adichtchev, V. K. Malinovsky, A. G. Ogienko, V. A. Drebushchak, A. Yu. Manakov, A. I. Ancharov, A. S. Yunoshev and E. V. Boldyreva, *J. Chem. Phys.*, 2012, **137**, 06510.
44 B. A. Zakharov, A. G. Ogienko, A. S. Yunoshev, A. I. Ancharov and E. V. Boldyreva, *CrystEngComm*, 2015, **17**, 7543.
45 S. Chan, J. Kendrick, M. A. Neumann and F. Leusen, *CrystEngComm*, 2013, **15**, 3799.
46 E. V. Boldyreva, *Cryst. Growth Des.*, 2007, **7**, 1662.
47 J. Ridout, L. S. Price, J. A. K. Howard and M. R. Probert, *Cryst. Growth Des.*, 2014, **14**, 3384.
48 M. Fisch, A. Lanza, E. Boldyreva, P. Macchi and N. Casati, *J. Phys. Chem. C*, 2015, **119**, 18611.
49 Y. Suzuki, G. Sazaki, T. Matsui, K. Nakajima and K. Tamura, *J. Phys. Chem. B*, 2005, **109**, 3222.
50 S. L. Price, *Chem. Soc. Rev.*, 2014, **43**, 2098.
51 J. Nyman and G. M. Day, *CrystEngComm*, 2015, **17**, 5154.
52 M. A. Neumann, J. van de Streek, F. P. A. Fabbiani, P. Hidber and O. Grassmann, *Nat. Commun.*, 2015, **6**, 7793.
53 M. Salvalaglio, T. Vetter, F. Giberti, M. Mazzotti and M. Parrinello, *J. Am. Chem. Soc.*, 2012, **134**, 172213.
54 M. Salvalaglio, F. Giberti and M. Parrinello, *Acta Crystallogr., Sect. C: Struct. Chem.*, 2014, **70**, 132.